

**Dynamics of entanglement and transport in one-dimensional systems with quenched randomness**Adam Nahum,<sup>1,2</sup> Jonathan Ruhman,<sup>2</sup> and David A. Huse<sup>3</sup><sup>1</sup>*Theoretical Physics, Oxford University, 1 Keble Road, Oxford OX1 3NP, United Kingdom*<sup>2</sup>*Department of Physics, Massachusetts Institute of Technology, Cambridge, Massachusetts 02139, USA*<sup>3</sup>*Department of Physics, Princeton University, New Jersey 08544, USA*

(Received 24 June 2017; published 16 July 2018)

Quenched randomness can have a dramatic effect on the dynamics of isolated 1D quantum many-body systems, even for systems that thermalize. This is because transport, entanglement, and operator spreading can be hindered by “Griffiths” rare regions, which locally resemble the many-body-localized phase and thus act as weak links. We propose coarse-grained models for entanglement growth and for the spreading of quantum operators in the presence of such weak links. We also examine entanglement growth across a single weak link numerically. We show that these weak links have a stronger effect on entanglement growth than previously assumed: entanglement growth is subballistic whenever such weak links have a power-law probability distribution at low couplings, i.e., throughout the entire thermal Griffiths phase. We argue that the probability distribution of the entanglement entropy across a cut can be understood from a simple picture in terms of a classical surface growth model. We also discuss spreading of operators and conserved quantities. Surprisingly, the four length scales associated with (i) production of entanglement, (ii) spreading of conserved quantities, (iii) spreading of operators, and (iv) the width of the “front” of a spreading operator, are characterized by dynamical exponents that in general are all distinct. Our numerical analysis of entanglement growth between weakly coupled systems may be of independent interest.

DOI: [10.1103/PhysRevB.98.035118](https://doi.org/10.1103/PhysRevB.98.035118)**I. INTRODUCTION**

A basic question about a many-body quantum system, closely related to its ability to thermalize, is how effectively quantum information spreads through it. The dynamical generation of quantum entanglement, following a quantum quench from a weakly entangled state, provides one window on information spreading [1–6]. Unitary dynamics typically generates correlations between increasingly distant degrees of freedom as time goes on. The resulting irreversible growth in the entanglement entropy of a subsystem reveals differences between integrable, nonintegrable, disordered, and many-body localized (MBL) [3,4,7] systems.

Complementary insight into information spreading comes from considering light-cone-like effects limiting the propagation of signals and disturbances through the system [8]. This leads to the question of how an initially local quantum operator spreads and becomes nonlocal under Heisenberg time evolution. Again there are important differences between clean and disordered systems.

In translationally invariant one-dimensional (1D) systems, entanglement growth and operator spreading are both typically associated with nonzero speeds [1,2,5,6,9]. By contrast, in the MBL phase, both entanglement growth [2–4,10,11] and operator spreading [12–18] are associated with length scales that grow only logarithmically in time.

This paper studies a third situation: 1D systems that are disordered, but are in the thermalizing phase. In 1D, quenched randomness can strongly affect transport and information spreading even in the thermal phase. This is because there can exist rare regions where disorder happens to be stronger than average, and which locally resemble the MBL phase.

These “Griffiths” regions act as bottlenecks or weak links, hindering the propagation both of conserved quantities and of quantum information. The effects on transport are fairly well understood: strong enough disorder leads to subdiffusive transport [19–21], as observed numerically [21–25]. (Certain rare-region effects have also been addressed experimentally [26].) Subballistic entanglement and signal propagation has been observed numerically in the Griffiths phase [23,27].

Here we provide long-wavelength pictures which expose the universal physics underlying entanglement growth and operator spreading in the Griffiths phase, and yield the universal scaling exponents and scaling forms governing these processes. In contrast to both clean systems and the MBL phase, we find that the length scales governing entanglement growth and operator growth (as measured by the so-called out-of-time-order correlator) scale with *different* powers of the time. In a certain sense, entanglement growth is parametrically slower than operator spreading in the Griffiths phase. We find that in a portion of the thermal Griffiths “phase” where the transport is diffusive and the operator spreading is ballistic, so in these two respects the rare regions do not change the disorder-free behavior, the entanglement growth remains subballistic due to the rare region effects. The transition from diffusive to subdiffusive transport is clearly exhibited in Ref. [25], although to show that required probing quite long length scales using matrix product methods. Our results say that the entanglement growth remains subballistic at this transition. Numerically probing this long-time entanglement behavior is a challenge that might be well beyond presently known methods and capabilities. The physics of this regime is weak links. Most models that have been numerically studied have uniform couplings and randomness only on the local fields

or potentials. To make this weak-link behavior more accessible in numerics, it may be worthwhile exploring models where the couplings are random, perhaps even with a power-law bare distribution of weak links.

We provide a long-distance picture for entanglement entropy growth in terms of an effective classical surface growth problem. The height of the growing “surface,”  $S(x)$ , is the amount of entanglement across a cut in the 1D system at position  $x$ ; the growth of the surface is deterministic, but it is affected by quenched randomness in the local growth rates. This picture is motivated by an analogy to a simpler quantum dynamics based on a random quantum circuit [6]. The basic assumptions are also substantiated independently, including with a semimicroscopic analysis of entangling across a Griffiths region.

The surface growth picture leads to the unexpected conclusion that entanglement growth is subballistic throughout the entire thermal Griffiths phase, i.e., whenever Griffiths regions locally resembling the MBL phase are possible. (This appears to require the absence of exact non-Abelian symmetries, as these appear to prohibit MBL [28–30].) We give expressions for the dynamical exponent governing the growth of the von Neumann entropy and for the probability distribution of this quantity at late times.

Turning to operator growth, we propose a very simple “hydrodynamic” picture for the out-of-time-order correlator in the Griffiths phase, making use of the random circuit results in Ref. [31] (see also Ref. [32]). We obtain a picture involving two separate diverging length scales at long times. In fact, we argue that in the Griffiths phase there are in general at least four separate dynamical exponents  $z$ , characterizing four length scales that can grow with time with different exponents: these are associated with entanglement growth ( $z_S$ ), with the spreading of an operator ( $z_O$ ), with the width of the “front” of the OTOC ( $z_W$ ), and with spreading of conserved quantities ( $z_C$ ). (See the table in Sec. V.) In particular, ballistic spreading of operators does not imply ballistic spreading of entanglement, contrary to previous suggestions.

Studying the thermal Griffiths phase leads naturally to questions about how two weakly coupled systems exchange quantum information. These questions are of general interest, outside the context of disordered systems. How do two weakly coupled quantum systems become entangled over time? How do operators localized in one of the systems spread across the weak link? We provide numerical and analytical results for generation of entanglement across the weak link, showing that the entanglement entropy is governed by a very simple scaling function and that the “weak link” can be characterized by a well-defined entanglement growth rate. (We investigate numerically how this growth rate depends on the strength of the weak coupling and on the index  $n$  of the Renyi entropy  $S_n$ .) We propose a simple scaling form for the out-of-time-order correlator of an operator which spreads across a weak link between two semi-infinite 1D chains.

## II. ENTANGLEMENT GROWTH

In this section, we study entanglement growth starting from a weakly entangled state: this could be the ground state of the pre-quench Hamiltonian in a quantum quench. The specific 1D

system does not matter at this stage, but an archetypal example is the Heisenberg spin chain with random couplings and fields,

$$H = \sum_i J_i \vec{S}_i \cdot \vec{S}_{i+1} + \sum_i h_i S_i^z. \quad (1)$$

(We could also consider a Floquet spin chain with effective discrete time dynamics.) Such chains will thermalize if the randomness is not too strong. However, thermalization may be slow as a result of weak links. These may be simply weak couplings where a single bond  $J_i$  is very weak. More robustly, the weak links may be due to extended Griffiths regions where the disorder happens to be more severe, so that MBL physics arises locally [21].

Moving to a coarse-grained description, let us label weak links by an index  $i$ , with a given weak link located at a position  $x_i$ . A key assumption is that each weak link has a well-defined local *entanglement rate*  $\Gamma_i$ , which is the rate at which entanglement is generated across the weak link in the absence of other weak links. We will give arguments supporting this assumption in Secs. VI and VII. The local entanglement rates are assumed to be independent random variables with a power-law distribution at small  $\Gamma$ :

$$P(\Gamma) \sim A \Gamma^a, \quad -1 < a < \infty. \quad (2)$$

The weak links are the tail of this distribution to small  $\Gamma$ . The exponent  $a$  depends on the strength of disorder and decreases as the many-body localization transition is approached, possibly approaching  $-1$  at the transition. The power-law form arises because the probability of a Griffiths region of length  $\ell$ , and the entangling rate associated with such a region, both decrease exponentially with  $\ell$  (Sec. VI). Or the power law might arise directly from the “bare” probability distribution of the couplings  $J_i$ . As usual, we will neglect the weak link’s nonzero spatial extent  $\ell$ : for Griffiths regions this grows only logarithmically as  $\Gamma \rightarrow 0$ , so is negligible compared to the lengthscales discussed below which grow as powers of  $\Gamma$ .

Consider a chain with open boundary conditions that is in a pure quantum many-body state, and let  $S(x, t)$  be the von Neumann entanglement entropy across a cut through the bond at position  $x$  at time  $t$ . Formally,

$$S(x, t) = -\text{Tr} \rho_{A_x}(t) \log \rho_{A_x}(t), \quad (3)$$

where the subsystem  $A_x$  contains the degrees of freedom to the left of  $x$  (Fig. 1). We could also consider a mixed state of the full system, in which case this is the von Neumann entropy of the subsystem to the left of the cut.

We will model the dynamics of  $S(x, t)$  as deterministic surface growth. In the next section, we will motivate this using a toy model for entanglement growth in the presence of weak links, but first we describe the consequences for the coarse-grained dynamics.

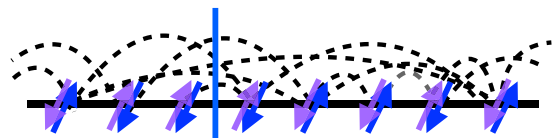


FIG. 1. Schematic: entanglement across a cut through bond at position  $x$ .

The surface growth picture takes into account two crucial physical constraints. First, the growth rate at a weak link  $i$ , which is at position  $x_i$ , is constrained by the local rate  $\Gamma_i$ . Second, the spatial slope of the entropy profile  $S(x,t)$  is constrained by the density of active degrees of freedom in the spin chain:

$$\partial S(x_i,t)/\partial t \leq \Gamma_i, \quad |\partial S(x,t)/\partial x| \leq s_{\text{eq}}. \quad (4)$$

Here,  $s_{\text{eq}}$  is the entropy density of the thermal state to which the system is locally equilibrating. The second inequality follows from subadditivity of the von Neumann entropy, together with the assumption that *local* reduced density matrices (for  $O(1)$  adjacent spins) thermalize at late times (no local high-entropy “hot spots”). In a lattice spin model at infinite temperature,  $s_{\text{eq}}$  is the logarithm of the local Hilbert space dimension per unit length; this version of the inequality follows rigorously from subadditivity. In the following, we will rescale  $x$  so that the inequality becomes

$$|\partial S(x,t)/\partial x| \leq 1. \quad (5)$$

If the system has any conserved densities, such as energy, that have a spatial distribution that is away from thermal equilibrium, then these equations for entanglement production are coupled to the transport equations for the conserved densities, and  $\Gamma_i$  and  $s_{\text{eq}}$  in general depend on the local densities. For simplicity, we will assume that any such conserved densities are close to equilibrium and it is only the entanglement that is far from equilibrium. (This is natural for a quench from an initial state with a spatial distribution of conserved quantities that is statistically homogeneous: at times much larger than microscopic timescales, but much smaller than  $L$ , the conserved density will locally be close to equilibrium, but the entanglement across a given cut can still be far from its equilibrium value.) More generally, since there are regimes where the transport is slower than the entanglement dynamics, in some circumstances the late time entanglement dynamics can be slowed due to being constrained by the more slowly relaxing conserved density (if this is sufficiently spatially nonuniform).

As a result of these inequalities, each weak link  $i$  imposes the constraint  $S(x,t) \leq S(x_i,0) + \Gamma_i t + |x - x_i|$ . We propose that at late times the entropy is essentially as large as it can be given these constraints:

$$S(x,t) = \min_i \{S(x_i,0) + \Gamma_i t + |x - x_i|\}. \quad (6)$$

The entanglement across a bond at  $x$  is therefore determined by a single locally “dominant” weak link. The spatial boundaries are taken into account by treating them as weak links with  $\Gamma = 0$ . For a pure state, the final profile at asymptotically late times, once the system has fully thermalized, is the pyramid  $S(x,t) = \min\{x, L - x\}$ . These formulas, of course, neglect subleading corrections (see Sec. II A); for example, we know that the entanglement near the center of the chain will depart from the maximal value by an  $O(1)$  correction even as  $t \rightarrow \infty$  [33].

Figure 2 shows growth according to the rule in Eq. (6). In the next section, we will see how it emerges at large lengths and timescales from a semimicroscopic toy model.

A simple optimization argument tells us how  $S(x,t)$  scales with time if we start from a pure product state with  $S(x,0) = 0$ . Let  $D$  be the typical distance to the dominant weak link at time  $t$ . The weakest link within this distance scale will have a rate

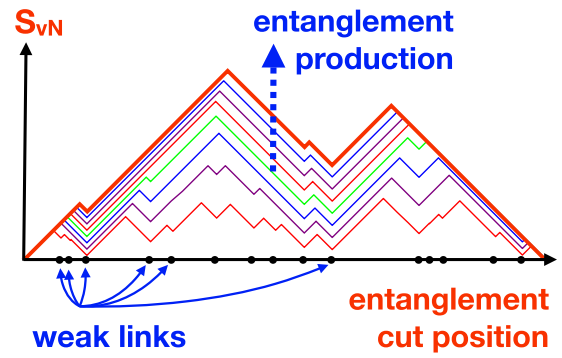


FIG. 2. Surface growth picture for entanglement  $S(x)$  across a cut at  $x$  in a finite chain, following Eq. (6). The lines show successive equally spaced times. Weak links with larger rates  $\Gamma$  are successively “dominated” by weaker links with smaller  $\Gamma$ . [This sample was generated with  $a = 0$ , see Eq. (2).]

of order  $\Gamma_{\min} \sim D^{-1/(a+1)}$ , so the two terms in  $\Gamma_i t + |x - x_i|$  will scale as  $D^{-1/(a+1)}t$  and  $D$ , respectively. Minimizing with respect to  $D$  gives

$$S(x,t) \sim t^{1/z_S}, \quad z_S = \frac{a+2}{a+1}. \quad (7)$$

The dynamical exponent  $z_S$  sets the typical lengthscale for entanglement at time  $t$ : for example, the typical time for the entanglement profile to saturate in a finite system of size  $L$  will be of order  $L^{z_S}$ . It also governs the typical distance to the locally dominant weak link,

$$D \sim t^{1/z_S}. \quad (8)$$

This is the lengthscale for the dynamical coarsening of the entanglement pattern visible in Fig. 2.

A key feature of Eq. (7) is that the entropy grows “subballistically” even for arbitrarily weak disorder, i.e.,  $z_S$  exceeds one for any finite  $a$ . This is despite the fact that operator growth is ballistic for large enough  $a$ , as we will explain in Sec. III. Equation (7) differs from earlier results which effectively assumed the timescale for entanglement saturation of a large chain was equal to a timescale associated with the weakest link in the chain [19,20]. These previous works took a viewpoint of the “spreading” of entanglement, while we now argue that this process is more accurately viewed as the constrained local *production* of entanglement. The situation with numerical studies of entanglement production (and its relation to operator spreading) in this Griffiths regime is still unclear: Ref. [27] reports exponents quite different from what we find here, but then their exponents also appear to be inconsistent with Ref. [34], which studies the entanglement of the unitary time evolution operator rather than of initial product states. It seems likely that the finite size effects are still very strong for the sizes that have been studied numerically.

Since  $S$  in Eq. (7) is the minimum of a set of uncorrelated random variables, it is straightforward to find its full probability distribution in the limit of an infinite chain initiated in a pure product state. If the density of weak links is  $\rho$  and the distribution of local rates is (2) at small  $\Gamma$ , the cumulative

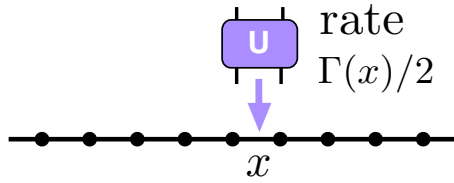


FIG. 3. Random circuit model: each bond  $x$  receives Haar-random unitaries at its own rate  $\Gamma(x)/2$ .

probability distribution at long time is

$$P(\text{entropy} > S) = \exp\left(-c \frac{S^{a+2}}{t^{a+1}}\right) \quad (9)$$

with (restoring the equilibrium entropy density  $s_{\text{th}}$ )

$$c = \frac{2A\rho}{s_{\text{th}}(a+1)(a+2)}. \quad (10)$$

The surface growth picture is restricted to the entanglement across a single cut; to generalize to regions with multiple endpoints, or to periodic boundary conditions, we may use the “directed polymer” description in Sec. II B.

### A. Random circuit model

Quantum circuit dynamics, with randomly chosen two-site unitaries, capture many universal features of entanglement growth in translationally invariant systems [6]. This setup is easily adapted to give a toy model for entanglement growth in the presence of weak links. This leads to a concrete surface growth problem defined on the lattice, from which the coarse-grained rule (6) can be seen to emerge in the scaling limit. This is not a derivation of the surface growth picture for isolated 1D systems with time-independent Hamiltonian or Floquet dynamics, whose microscopic dynamics are very different from the toy model; however, it motivates the surface growth picture, some of whose predictions can subsequently be checked by other means.

Consider a chain of spins, each with a large local Hilbert space dimension,  $q \gg 1$ . The chain is initially in an unentangled product state. Random two-site unitaries are then applied to adjacent spins in a Poissonian fashion, at rates  $\frac{1}{2}\Gamma(x)$  that depend on the bond  $x$  (Fig. 3). These rates are distributed at small  $\Gamma$  as in Eq. (2).

At large  $q$ , the dynamics of the entanglement  $S(x, t)$  across bond  $x$  maps exactly to a classical surface growth model [6]. We absorb a factor of  $\log q$  into the definition of  $S$  (by defining the von Neumann entropy using a logarithm base  $q$ ). The entanglement  $S(x, t)$  then obeys a very simple dynamical growth rule: each time a unitary is applied to bond  $x$ ,  $S(x, t)$  increases to the maximal value allowed by the general constraint that  $S(x, t)$  can exceed  $S(x \pm 1, t)$  for the neighboring bonds by at most 1. With this growth rule, the differences between adjacent heights are always  $\pm 1$  at late times [6].

The resulting dynamics is microscopically stochastic. However, we may neglect the noise-induced fluctuations, since they are negligible in the long-wavelength limit.

First, take  $\Gamma$  to be constant (no weak links), and consider the growth of a region whose coarse-grained slope  $\partial S/\partial x$  is

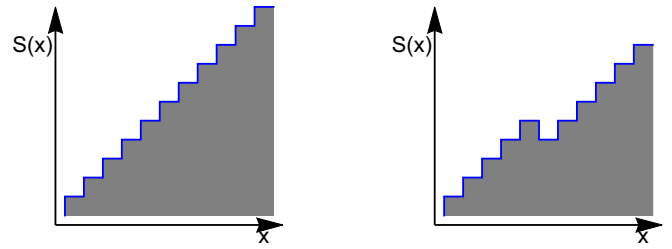


FIG. 4. (Left) Maximum possible slope for the entanglement profile in the quantum circuit model,  $\partial S/\partial x = 1$ . (Right) A staircase with a defect. After coarse-graining, a finite density  $\rho$  of defects results in a slope  $\partial S/\partial x = 1 - 2\rho$ .

constant. If the surface is flat,  $\partial S/\partial x = 0$ , the growth rate is  $\Gamma/4$  [35]. The important regime for us will instead be where the slope  $|\partial S/\partial x|$  is close to the maximal value of unity. Microscopically, this means that the surface is close to the perfect staircase configuration shown in Fig. 4 (left). Note that the growth rate vanishes in this configuration. However, when  $|\partial S/\partial x|$  is slightly smaller than unity, there is a small density  $\rho$  of “defects” in the staircase, involving a local minimum of the height, see Fig. 4 (right). These defects allow growth. Each time a unitary hits a defect, the local height increases by two units. The coarse-grained growth rate is thus  $\partial S/\partial t \simeq \rho\Gamma$ . The coarse-grained slope is given by  $|\partial S/\partial x| = 1 - 2\rho$ , so

$$\frac{\partial S}{\partial t} \simeq \frac{\Gamma}{2} \left(1 - \left|\frac{\partial S}{\partial x}\right|\right). \quad (11)$$

Note that, microscopically, each time a unitary hits a defect, the defect moves up the staircase by one step, so defects run up the staircase at an average speed  $\Gamma/2$ . The growth rate  $\partial S/\partial t$  can be also thought of as (twice) the “current” of these defects.

Next, consider entanglement growth in a system with a single weak link at the origin, with rate  $\Gamma_1 \ll \Gamma$ . At a typical time  $t$ , the local configuration resembles Fig. 5 (left). Microscopically, the weak bond is almost always a local minimum of the height profile. Unitaries are applied there at a rate  $\Gamma_1/2$ , causing growth at rate  $\Gamma_1$ . Each such event launches one defect up each staircase on the two sides of the weak link. The growth rate of the adjacent regions is therefore set by the growth rate at the weak link,  $\partial S/\partial t = \Gamma_1$ . The coarse-grained slope of the adjacent regions is fixed using (11):  $|\partial S/\partial x| = 1 - 2\Gamma_1/\Gamma$ . For small  $\Gamma_1$ , the deviation of the slope from unity is small. Neglecting this deviation,

$$S(x, t) \simeq \min\{\Gamma_1 t + |x|, \Gamma t/4\}, \quad (12)$$



FIG. 5. Growth at a weak link location (random circuit model). Unitaries are applied at the weak link at a small rate  $\Gamma_1$ . Each such event increases the height at the origin by two units. Two “defects” then travel up the sides of the double staircase at an average speed  $\Gamma/2$ .

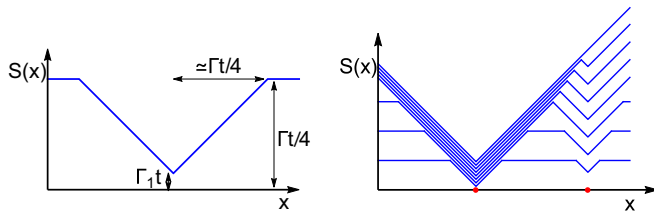


FIG. 6. (Left) Entanglement growth around a weak link characterized by a small rate  $\Gamma_1$ . (Right) Entanglement growth around a pair of weak links, showing how the weaker link dominates at late times. The figure shows eight equally spaced times.

when the initial state is a pure product state. This profile is shown in Fig. 6 (left). The weak link influences a region of size  $\simeq \Gamma t/4$  on either side.

It is straightforward to generalize to multiple weak links. Consider two with rates  $\Gamma_1$  and  $\Gamma_2$  that are separated by a distance  $l$  [Fig. 6 (right)]. We take  $\Gamma_1 < \Gamma_2 \ll \Gamma$ . The regions of influence of the two weak links meet at a time  $\simeq 2l/\Gamma$ , giving a profile with a central peak. The region of influence of the weaker link then gradually expands at the expense of the stronger link. At time  $t \simeq l/(\Gamma_2 - \Gamma_1)$ , the central peak hits the link with the rate  $\Gamma_2$  and disappears. Subsequently, the link with the larger rate has no effect on the coarse-grained configuration, being “dominated” by the weaker link. (The link with rate  $\Gamma_2$  does not affect the slope, or equivalently the density of defects, in this regime, except precisely at its location: the flow of defects is limited only by the slower rate  $\Gamma_1$ .) Again, we may write

$$S(x, t) \simeq \min\{\Gamma_1 t + |x - x_1|, \Gamma_2 t + |x - x_2|, \Gamma t/4\}. \quad (13)$$

The same logic extends to arbitrary numbers of weak links. The  $\Gamma t/4$  term can be dropped since at large times every point  $x$  is within the domain of influence of some weak link. This gives Eq. (6).

We may also quantify the subleading corrections to Eq. (6): the average gradient  $|\partial S/\partial x|$  of the straight sections<sup>1</sup> is reduced from the maximal value of unity by an amount of order  $D^{-1/(a+1)}$  when  $a > 0$  and of order  $D^{-1}$  when  $a < 0$ . Since  $D \sim t^{1/z_s} \gg 1$ , these corrections are indeed small.

### B. “Minimal cut” interpretation

There is a general relationship between surface growth in 1+1D and the statistical mechanics of a directed polymer in a two-dimensional environment [36]. The results discussed above may also be understood in this language, and this allows them to be generalized to more complex geometries.

<sup>1</sup>For large  $t$ , the profile consists of staircases of typical length  $D \sim t^{1/z_s}$  with almost-maximal coarse-grained  $|\partial S/\partial x|$ . The minima between such staircases are weak links with typical strength  $\Gamma_{\min} \sim D^{-1/(a+1)}$  [see above Eq. (7)]. The gradient at position  $i$  is less than the maximum by  $O(\Gamma_{\min}/\Gamma_i)$ . Summing this, the total height of the staircase is reduced from that of a perfect staircase by  $\Delta S$  of order  $\Gamma_{\min} \sum_{i=1}^D \Gamma_i^{-1}$  (note  $\Gamma_i \geq \Gamma_{\min} + x/t$ ), which gives the scaling in the text.

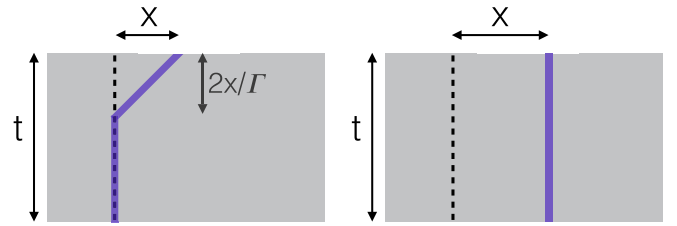


FIG. 7. Minimal cut configurations determining  $S(x, t)$  in an infinite system with a single weak link of strength  $\Gamma_1$ . The grey patch represents the unitary circuit and the thick line represents the (coarse-grained) minimal cut: (left) for  $x < \frac{\Gamma t (1-4\Gamma_1/\Gamma)}{4}$  and (right) for  $x > \frac{\Gamma t (1-4\Gamma_1/\Gamma)}{4}$ .

In the context of entanglement, the directed polymer may be viewed as a coarse-grained “minimal cut” through a unitary circuit representing the dynamical evolution [6]. We briefly summarize the main features of this coarse grained picture as it applies to the random circuit model. In the present case, with weak links, we obtain a directed polymer subject to pinning by vertical defect lines [37].

The entanglement  $S(x, t)$  is given by the “energy” of a minimal energy cut which splits the space-time slice into two disconnected pieces—see Fig. 7. (In this section we treat the time  $t$  as a spatial dimension.) One endpoint of this cut must be at position  $x$  on the top boundary, and the cut must disconnect the parts of the top boundary to the left and right of  $x$ . In an infinite system, this means that the other endpoint of the cut must be at the bottom boundary. In the absence of weak links, the minimal energy such cut is vertical, and the energy per unit height is  $\Gamma/4$  (in the notation of Ref. [6] this is the entanglement rate  $v_E$ ). In a finite system, the cut can terminate on the left- or right-hand spatial boundary.

To begin with it is sufficient to consider only horizontal and vertical cuts. The energy of a horizontal cut is equal to its extent in the  $x$  direction. If we consider  $S(x, t)$  in a clean semi-infinite system with a boundary at position 0, the minimal cut is vertical and of energy  $\Gamma t/4$  for early times, while at late times the horizontal cut with energy  $x$  is favorable; this gives  $S(x, t) = \min\{\Gamma t/4, x\}$ .

A single weak link corresponds to a vertical defect line where the energy density per unit height is reduced and equal to  $\Gamma_i$ . For large  $t$ , it is worthwhile for the polymer to travel a large horizontal distance to take advantage of this favorable energy density. It must of course “pay” in energy for the nonvertical section required to reach the defect. For a crude picture, we can consider only horizontal and vertical segments; it is easy to see that in an infinite system we then recover Eq. (12).

In more detail, the energy of a segment of horizontal extent  $x$  remains equal to  $x$  even if the segment is at a finite angle to the horizontal, so long as this angle is small enough<sup>2</sup> (this is true for slopes  $\geq 2/\Gamma$ ). This means that the true minimal

<sup>2</sup>This can be seen from the microscopic picture of the polymer as a “minimal cut” through the large- $q$  unitary circuit. The energy of the polymer is equal to the number of bonds it cuts. A horizontal cut of length  $x$  cuts  $x$  bonds. This horizontal cut can be deformed to one with a finite coarse-grained slope, with the same energy, so long as

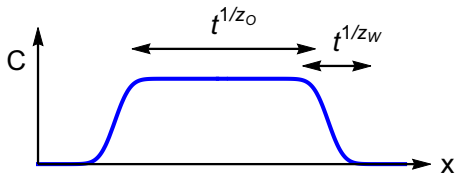


FIG. 8. Definition of dynamical exponents  $z_O$  and  $z_W$  governing the size of a spreading operator and the size of the front [as measured using the OTO correlator  $C(x,t)$ , Sec. III]. The front is only well-defined in the weak-disorder regime ( $a > 1$ ), where  $z_O = 1$  and  $z_W < 1$ .

cut configuration for small  $x$  is as shown in Fig. 7. This corresponds to taking subleading corrections in the slope of  $S(x)$  into account, and gives  $S(x,t) = \Gamma_1 t + (1 - 2\Gamma_1/\Gamma)|x|$  in agreement with the previous section.

This picture may be extended to multiple weak links. The typical transverse excursion for a given cut is of order  $D \sim t^{1/z_S}$ , so much smaller than  $t$  [Eq. (8)]. It may also be extended to a region with multiple endpoints. Consider the entanglement of a finite region of length  $x$  in an infinite system. At early times, the minimal cut configuration involves two disconnected cuts, giving an entanglement of order  $t^{1/z_S}$ , which is the sum of two independent random variables distributed as in Eq. (9). Once this becomes equal to  $x$ , a configuration with a single horizontal cut becomes favorable.

### III. OPERATOR SPREADING

Heisenberg time evolution will transform a local operator, for example, the Pauli matrix  $X_0$  located at the origin in a spin chain, into a complex object  $X_0(t) = U(t)^\dagger X_0 U(t)$ , which acts nontrivially on many sites. The spatial extent of this growing operator may be quantified using the commutator with a local operator at site  $x$  [8]. In particular, one can define the recently much-studied object [9,12–18,27,38–54]

$$C(x,t) = -\frac{1}{2} \text{Tr} \rho_\beta [X_0(t), X_x]^2, \quad (14)$$

where  $\rho_\beta$  is the density matrix  $e^{-\beta H}/Z$  at the appropriate temperature. Expanding the squared commutator gives the “out-of-time-order” (OTO) correlator

$$C(x,t) = 1 - \text{Tr} \rho_\beta X_0(t) X_x X_0(t) X_x. \quad (15)$$

$C(x,t)$  is of order one in a spatial region whose size grows with  $t$ , and  $C(x,t)$  vanishes far outside this region. In translationally invariant systems the size of the operator, as measured by  $C$ , grows ballistically with a speed  $v_B$  known as the butterfly speed.

Here we address the size and “shape” of spreading operators in the thermal Griffiths phase (see Fig. 8). For simplicity, we consider the case  $\beta = 0$ , but we do not expect this to change the basic results. We determine dynamical exponents  $z_O$  and  $z_W$ , which give respectively the typical size  $t^{1/z_O}$  of the operator at time  $t$  and the typical size  $t^{1/z_W}$  of its “front”—the region in which  $C$  is of order one, but smaller than the saturation

the slope is  $\geq 2/\Gamma$  (this is the typical vertical distance that the cut can travel before being blocked by a unitary).

value. The shape of the operator turns out to be qualitatively different for weak and strong disorder. For weak disorder  $z_W > z_O$ ; in this regime, the front is much smaller than the “plateau” region in which  $C$  has saturated to its maximum value. Conversely, for strong disorder,  $z_W = z_O$ , so that  $C$  does not have a well-defined plateau when lengths are scaled by the spreading length.

Our starting point is a picture for operator spreading in 1D systems developed on the basis of calculations in random circuits in Ref. [31] (see also parallel work [32]). It is shown there that for  $x > 0$  and for long times, we may write (we switch to a continuum notation)

$$C(x,t) = \int_x^\infty dx' \rho(x',t), \quad (16)$$

where  $\rho(x,t)$  is a conserved density

$$\int_0^\infty \rho(x,t) = 1, \quad (17)$$

and where—in a random circuit without weak links— $\rho(x,t)$  behaves essentially like the probability density of a random walker with a bias in favor of rightward steps. The average speed  $v_B$  of the walker sets the butterfly velocity. For  $x < v_B t$ , the bulk of the density is within the range of integration in (16), yielding  $C(x,t) \simeq 1$ ; for  $x > v_B t$ , the density is mostly outside the range of integration, giving  $C(x,t) \simeq 0$ . The transition region broadens diffusively, with width  $\sim \sqrt{t}$ . This picture in terms of the density  $\rho$  generalizes very naturally to the situation with weak links, where  $v_B$  is no longer necessarily nonzero.

Let us briefly summarize the meaning of the density  $\rho$  [31]. First, write the spreading operator at time  $t$  in the basis of products of Pauli matrices,

$$X_0(t) = \sum_S a_S(t) \mathcal{S}. \quad (18)$$

Here,  $\mathcal{S}$  is a string (product) of Pauli matrices at different sites. These strings satisfy

$$\text{Tr} \rho_\infty \mathcal{S} \mathcal{S}' = \delta_{\mathcal{S} \mathcal{S}'}, \quad (19)$$

and since  $\text{Tr} \rho_\infty X_0(t)^2 = 1$  we have  $\sum_S a_S(t)^2 = 1$ . The density  $\rho(x,t)$  is the “fraction” of strings that *end* at position  $x$  (a string  $\mathcal{S}$  ends at  $x$  if  $x$  is the rightmost site at which it acts nontrivially):

$$\rho(x,t) = \sum_{\substack{S \\ \text{(ends at } x)}} a_S^2. \quad (20)$$

The density  $\rho(x,t)$  is evidently conserved and is normalized to one,  $\sum_x \rho(x,t) = 1$ , despite the fact that the *number* of distinct strings contributing to this density grows exponentially with time.

Consider  $C(x,t)$  for  $x > 0$ . Inserting the expression (18) shows that  $C(x,t)$  is

$$C(x,t) = 2 \sum'_S a_S^2, \quad (21)$$

where the primed sum includes only those strings whose commutator with  $X_x$  is nontrivial. Strings whose right endpoint is at a position to the left of  $x$  cannot contribute to this sum, but an  $O(1)$  fraction of those whose right endpoint is to the

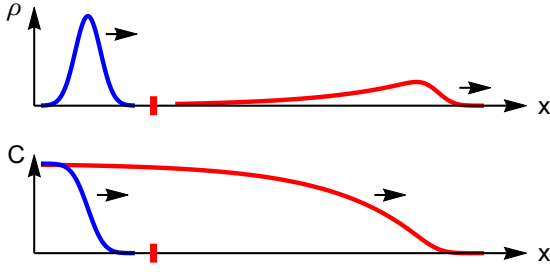


FIG. 9. Operator spreading caused by passage through a weak link (schematic). (Top) The spreading of the “wave packet”  $\rho(x,t)$  [Eq. (16)]. (Bottom) The corresponding spreading of the front of the commutator  $C(x,t)$  [Eq. (14)].

right of  $x$  do contribute. Specifically, we expect<sup>3</sup> this fraction to be  $1/2$ , giving (16). In a random circuit without weak links,  $\rho(x,t)$  may be argued to satisfy a noisy diffusion equation with bias [31].

This motivates the following picture for a system whose dynamics is deterministic but spatially random. We first consider the spreading of an operator through a single weak link, and then generalize to a Griffiths chain with many weak links.

#### A. Operator spreading across one weak link

Consider two regions in which operators spread at speed  $v_B$ , separated by a weak link characterized by a very small rate  $\Gamma$ . For simplicity, we think of the weak link as a weak bond at position  $x = 0$ , and consider its effect on the rightward front of an operator which is initially localized in the leftward part of the system.

First, the density  $\rho(x,t)$  advances to the weak link, which we take to be located at position  $x = 0$ , reaching the weak link at time  $t_*$ . We neglect the diffusive spreading in  $\rho$  prior to passing through the weak link. It is easy to restore this effect in what follows by a more detailed treatment of biased diffusion on a chain with weak links, but it is not important for the scaling exponents below. The density then leaks through at a rate  $\Gamma$ , so

$$\rho(0^-, t) = e^{-\Gamma(t-t_*)}, \quad (22)$$

where  $0^-$  is the lattice site to the left of the weak link. The density on the other side of the weak link is

$$\rho(0^+, t) = \frac{\Gamma}{v_B} e^{-\Gamma(t-t_*)}. \quad (23)$$

(Walkers hop across at rate  $\Gamma$ , and are whisked away at speed  $v_B$ .) Since we neglect spreading of  $\rho$  within the homogeneous region, the density to the right of the weak link is related to the above by  $\rho(x,t) = \rho(x - v_B t)$ : for  $0 < x < v_B(t - t_*)$  we have

$$\rho(x,t) = \frac{\Gamma}{v_B} \exp \left\{ \frac{\Gamma}{v_B} [x - v_B(t - t_*)] \right\}. \quad (24)$$

At times  $\gtrsim 1/\Gamma$  (but small compared to  $v_B^2/\Gamma^2 D$ , when diffusive spreading becomes comparable), the packet  $\rho(x)$  is of width  $\sim v_B/\Gamma$  and of height  $\Gamma/v_B$  [see Fig. 9 (top)].

#### B. Operator spreading across many weak links

To understand spreading across multiple weak links, it is useful to think of each one as performing a linear transformation on the “wave packet”  $\rho(x,t)$ . We go into a frame moving at speed  $v_B$ . The foregoing tells us that if the initial wave packet is

$$\rho_0(x) = \delta(x - x_0), \quad (25)$$

then the new wave packet is (we define  $\gamma = \Gamma/v_B$ )

$$\rho_1(x) = \gamma e^{\gamma(x-x_0)} \quad (x < x_0). \quad (26)$$

In other words, by linearity,

$$\rho_1(x) = \gamma \int_0^\infty dy e^{-\gamma y} \rho_0(x+y). \quad (27)$$

This transformation may be iterated.<sup>4</sup> It preserves the normalization of  $\rho$  and it acts in a simple way on the mean and variance. If the  $k$ th weak link encountered has strength  $\gamma_k$ ,

$$\begin{aligned} \langle x \rangle_{k+1} &= \langle x \rangle_k - \gamma_k^{-1}, \\ \langle x^2 \rangle_{k+1} &= \langle x^2 \rangle_k + \gamma_k^{-2}. \end{aligned} \quad (28)$$

#### C. Operator spreading in the Griffiths phase

Next, let us consider the leading edge of the commutator as it passes through a sequence of weak links  $\Gamma_k$ , with a probability distribution  $P(\Gamma) \sim \Gamma^a$ . (In this section, we use a unit of length such that the density of weak links is unity.) There are three separate questions: (i) how far has the leading edge traveled at time  $t$ ? (ii) What is the typical width of the leading edge after a time  $t$ , *within* a given sample, i.e., for a given realization of the quenched disorder? (iii) How much variation in the position of the leading edge is there between *different* disorder realizations?

After traveling a distance  $x$ , the wave packet has passed through  $O(x)$  weak links. From the formula for the mean, the position of the wave packet is

$$x \simeq v_B t - \sum_{k=1}^x \gamma_k^{-1}, \quad (29)$$

where we have made the approximation that all parts of the wave packet have passed through the same number of weak links. (This simplification does not change the scaling of  $x$ , but must be considered more carefully for the fluctuations below.) The scaling of the sum in (29) depends on the value of  $a$ . In the regime  $a > 0$ , the sum is proportional to the number of terms,

<sup>3</sup>A given string can either have  $X, Y, Z$  or  $1$  at site  $x$  (two of which commute with  $X$ ), and we expect all options to be equally likely [31] deep in the interior of the operator.

<sup>4</sup>For example, for one choice of initial condition, iterating with the same value of  $\gamma$  gives  $\rho_k = \gamma \frac{(-\gamma x)^k}{k!} e^{\gamma x}$  ( $x < 0$ ), which becomes Gaussian for large  $k$ .

whereas for  $a < 0$  it is dominated by the smallest  $\gamma$ , which is of order  $x^{-1/(a+1)}$ . This gives

$$a > 0: \quad x \sim t, \quad z_O = 1, \quad (30)$$

$$a < 0: \quad x \sim t^{a+1}, \quad z_O = 1/(a+1), \quad (31)$$

where we have introduced the dynamical exponent  $z_O$  governing the size of a spreading operator.

Now let us estimate the spreading of the wave packet  $\rho(x,t)$  within a given sample. The variance formula (28) gives

$$\text{width}^2 \sim \sum_{k=1}^x \gamma_k^{-2}. \quad (32)$$

This formula will give the correct scaling in the regime where all parts of the wave packet have passed through  $O(x)$  links. This is the case for  $a > 0$ , where (32) gives a width much smaller than  $x$ . Interestingly, there are two distinct behaviors within the  $a > 0$  regime: for  $a > 1$  the sum is of order  $x$ , while for  $0 < a < 1$ , it is dominated by the minimal element:

$$a > 1: \quad x \sim t, \quad \text{width} \sim t^{1/2}, \quad (33)$$

$$0 < a < 1: \quad x \sim t, \quad \text{width} \sim t^{1/(a+1)}. \quad (34)$$

When  $a < 0$ , naive application of the variance formula gives width  $\gg x$ , showing that the approximation that all parts of the wave packet have traveled through  $O(x)$  weak links breaks down. In this regime, we expect simply that width  $\sim x$ , i.e.,

$$a < 0: \quad x \sim t^{a+1}, \quad \text{width} \sim t^{a+1}. \quad (35)$$

To see this, note that at time  $t$  some of the wave packet will have passed through the weakest nearby link, which is at distance  $x \sim t^{a+1}$  and has rate  $\gamma \sim 1/t$ , but some of the wave packet will still be held up by the second weakest nearby link, which is an  $O(1)$  fraction of the distance away.

Putting these results together,

$$a > 1: \quad x \sim t, \quad \text{width} \sim t^{1/2}, \quad (36)$$

$$0 < a < 1: \quad x \sim t, \quad \text{width} \sim t^{1/(a+1)}, \quad (37)$$

$$a < 0: \quad x \sim t^{a+1}, \quad \text{width} \sim t^{a+1}. \quad (38)$$

These formulas define a dynamical exponent  $z_W$  governing the width of the front of a spreading operator.

So far, we have considered the width within a given sample. Sample-to-sample variations in the front position are even more simply understood using (29). We find that in all regimes they scale with the same power of  $t$  as the width of the front within a given realization.

The exponents above are written in terms of the parameter  $a$  governing the distribution of weak link timescales. In using the same value of  $a$  for operator spreading and for entanglement spreading, we are making the natural (but unproven) assumption that the timescales for entanglement growth and operator spreading are of the same order for a severe weak link.

There is a relationship between the growth of the second Renyi entropy and the spreading of the operators appearing in an expansion of the reduced density matrix, which has been used to give heuristic pictures for entanglement growth [55,56]. Nevertheless, the growth “speed” associated with

entanglement is in general smaller than that for the spreading of operators, even in clean systems [6,56]. The Griffiths phase is an extreme example, where the two length scales grow with different powers of time.

To summarize, operators have a well-defined front and a nonzero butterfly velocity only when  $a > 0$ . In all regimes the width of the front increases with time, and there is a change in the exponent governing this width at  $a = 1$ . The various dynamical exponents are summarized below in Table I.

#### D. Operator entanglement

We may also consider the entanglement of a spreading operator, viewing the operator as a state in a “doubled” system [57]. The growth of this operator entanglement within the region in between the two “fronts” of the spreading operator is governed by essentially the same physics as that governing the growth of the entanglement of states. Thus we expect the operator entanglement to grow with dynamic exponent  $z_S$ . Since  $z_S > z_O$  for all allowed finite  $a$  within  $-1 < a < \infty$ , the entanglement  $S_{\text{op}}$  across the midpoint of a spreading operator is less than “volume law” as long as it is spreading, where we call the distance  $\ell$  between the two fronts the operator’s “volume”:  $S_{\text{op}} \sim \ell^{z_O/z_S}$ . Interestingly, this exponent is nonmonotonic. It is minimal at  $a = 0$  (assuming that timescales are characterized by a single exponent  $a$ ), and the volume-law exponent of unity is recovered in both limits,  $a \rightarrow \infty$  and  $a \rightarrow -1$ . Once the operator reaches the ends of the chain it can then become volume-law entangled.

#### IV. CONSERVED QUANTITIES

Here we revisit the dynamics of conserved quantities in the Griffiths phase, considered previously in Refs. [19–21], in order to compare with the spreading of operators and entanglement. We recover the dynamical exponent found previously for conserved quantities:

$$z_C = \min \left\{ 2, \frac{a_C + 2}{a_C + 1} \right\}. \quad (39)$$

Here,  $a_C$  is the exponent governing the distribution of rates for “hopping” of a given conserved quantity  $C$  across a weak link [cf. Eq. (2)]. The simplest assumption would be that there is a single weak link exponent  $a = a_C$  for both entanglement and transport, i.e., that (asymptotically) a given weak link is characterized by a single long timescale. This must be investigated further. It is natural to expect at least that  $a \geq a_C$ : the hopping of (say) a conserved charge across the weak link will generically induce  $O(1)$  entanglement, so the rate for entanglement production should not be parametrically smaller than that for conserved quantities. However, we may have  $a_C < a$ , and we may have distinct  $a_{C_S}$ , and therefore distinct  $z_{C_S}$ , for distinct conserved charges  $C$ .<sup>5</sup> Indeed, recent

<sup>5</sup>If there are several exponents  $a_C$ , the corresponding conserved charges  $C$  may be nontrivial linear combinations of those corresponding to the physical conservation laws, unless this is prevented by other symmetries. (These may be symmetries that hold exactly, or symmetries that hold statistically, i.e., on average.) That is, distinct



numerical work using long chains argues for a regime in the disordered XXZ model where energy transport is diffusive but charge transport is subdiffusive [58]. As we discuss at the end of this section, it is also possible to artificially design a chain with a  $U(1)$  charge for which  $a_{\text{charge}}$  is clearly smaller than both  $a$  and  $a_{\text{energy}}$ , although this example involves a power law distribution of *microscopic* weak links so may not be relevant to typical models in the Griffiths phase. In the following, we will neglect these subtleties and denote the relevant weak link exponent by  $a$  without a subscript.

Since the system locally looks thermal at late times, we may treat the dynamics of conserved quantities as a classical random walk—say on a 1D lattice, in continuous time—which is “bottlenecked” by weak links. We treat the weak links as bonds where the hopping rate is small. This setup preserves detailed balance.

For weak disorder, the dynamics is diffusive. To see when diffusive scaling breaks down, consider two adjacent weak links with  $\Gamma \leq \Gamma_0$ . Their interior defines a box of typical size

$$\Delta \sim \Gamma_0^{-(a+1)}. \quad (40)$$

Now, compare the time for a diffusing particle to cross this box,  $t_{\text{diff}} \sim \Delta^2$ , with the time for which the particle is detained by a single weak link of strength  $\Gamma_0$ . Once the walker reaches the weak link it must revisit it  $O(1/\Gamma_0)$  times before it succeeds in hopping across. By standard diffusive scaling, the time required for this number of revisits is  $t_{\text{traverse}} \sim 1/\Gamma_0^2 \sim \Delta^{2/(a+1)}$ . When  $a > 0$ , we have  $t_{\text{traverse}} \ll t_{\text{diff}}$ , and we expect diffusive scaling to be stable. On the other hand, when  $a < 0$  the two weak links trap the walker inside the box for much longer than  $t_{\text{diff}}$ . In this regime  $t_{\text{traverse}}$  will be of the same order as the time required to explore the box “ergodically.” The rate to cross one of the weak links is then the product of the fraction of the time spent adjacent to the weak link, namely  $1/\Delta$ , with the  $O(\Gamma_0)$  rate at the weak link. The typical time required to escape the box is therefore

$$t \sim \Delta/\Gamma_0 \sim \Delta^{(a+2)/(a+1)}. \quad (41)$$

This gives the dynamical exponent quoted above. This exponent agrees with the random walk model of Ref. [20], but the behavior of trajectories is different.<sup>6</sup>

The transition between diffusive and subdiffusive spin transport has been observed numerically in a disordered Heisenberg chain [25]; see also Refs. [21–24]. The transition between diffusive and subdiffusive energy transport has been observed in Refs. [58,59].

conserved quantities (for example, energy  $E$  and charge  $n$ ) may “mix” (this mixing is forbidden in the presence of the symmetry  $n \rightarrow -n$ ). This may be relevant to the regime of positive magnetization in Ref. [58].

<sup>6</sup>In the regime  $a < 0$ , a walker takes a time of order  $L/\Gamma_{\text{min}}$  to traverse a sample of size  $L$ , where  $\Gamma_{\text{min}}$  is the typical rate of the weakest link in the sample. In the above model this timescale is associated with trajectories that traverse the weak link  $O(1)$  times (this is consistent with the detailed balance requirement that in a closed chain all sites are visited equally in the limit of long times), whereas in the model of Ref. [20] it is associated with trajectories that traverse the weak link  $O(L)$  times.

TABLE I. Dynamical exponents governing lengthscales for entanglement growth ( $z_S$ ); spreading of conserved quantities ( $z_C$ ); spreading of quantum operators under Heisenberg time evolution ( $z_O$ ); width of the “front” of a spreading operator ( $z_W$ ). Here, we assume a single exponent  $a$  governs the distribution of timescales [see Eq. (2)] for the various processes at a weak link, see text.

	$-1 < a < 0$	$0 < a < 1$	$1 < a$
$z_S$		$(a+2)/(a+1)$	
$z_C$	$(a+2)/(a+1)$		2
$z_O$	$1/(a+1)$		1
$z_W$	$1/(a+1)$	$a+1$	2

If a quantum quench starts from a sufficiently inhomogeneous initial state, the relaxation of conserved quantities will affect the growth of entanglement. An extreme example is a 1D spin chain, with conserved  $S_z$ , which starts in a domain wall state with fully polarized up spins on the left and fully polarized down spins on the right. Since a polarized region has trivial dynamics, entanglement can only be generated in the growing central region where the polarization has been destroyed. For an initial state with only *short-range* correlated randomness in conserved quantities (i.e., a statistically homogeneous state), the local expectation value of the conserved quantity will relax to equilibrium with fluctuations of order  $t^{-1/2z_C}$ . These fluctuations will lead to fluctuations in the local entangling rates  $\Gamma$  for the weak links, but these will be negligible at late times.

Above we mentioned that at least in some circumstances we can have  $a_{\text{charge}} < a, a_{\text{energy}}$  (Ref. [58] contains numerical evidence for a model with  $z_{\text{charge}} > z_{\text{energy}}$ ). Here is a proof of principle argument for this possibility in a somewhat contrived model. Consider a chain with a conserved  $U(1)$  charge and with Hamiltonian  $H = H_1 + H_2$ . The terms in  $H_1$  are unable to move charge, but they give nontrivial dynamics and energy transport. We assume there are multiple states available at each site, regardless of the value of the charge there; concretely, the chain could involve, say, hard-core bosons that carry the spin, plus an additional Ising spin at each site to allow nontrivial dynamics regardless of the distribution of charge.  $H_2$  is the charge hopping. The hopping amplitudes are taken to be randomly distributed with a distribution with a power-law tail near zero, giving a power-law distribution of *microscopic* weak links for charge transport. We expect then that  $a_{\text{charge}}$  can be driven arbitrarily close to the minimal value  $-1$  by varying the microscopic hopping distribution. However, energy transport and entanglement generation can be accomplished by the terms in  $H_1$ , so we expect  $a_{\text{energy}}$  and  $a$  to exceed  $a_{\text{charge}}$  in this limit.

## V. DYNAMICAL EXPONENT SUMMARY

The dynamical exponents we have found are summarized in Table I, under the assumption (see caveats in Secs. III C and IV) that the long timescales characterizing a weak link are distributed with the same power law.

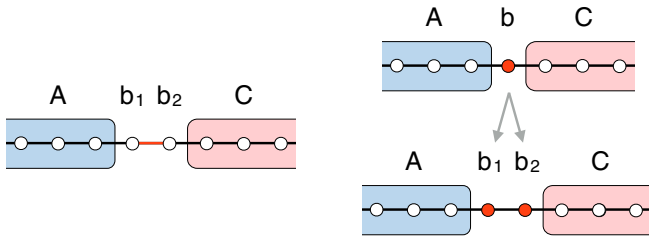


FIG. 10. Two types of microscopic weak link. Left: an infinite spin chain with a weak bond connecting spins  $b_1$  and  $b_2$ . (Top right) A chain in which the  $Z$  component of spin  $b$  is almost conserved. This can be mapped to a chain with a weak bond by duplicating  $b$  (bottom).

## VI. BOUNDING ENTANGLEMENT GROWTH ACROSS A GRIFFITHS REGION

In previous sections we assumed that a Griffiths region could be characterized by a local entanglement growth rate,  $\Gamma$ , which vanishes as the region becomes large. Here, we show analytically that the rate for entanglement growth across a Griffiths region is exponentially slow when the length  $\ell$  of the Griffiths region is large.

We will start by considering a trivial kind of weak link—a weak bond in a spin chain. For this simple case, a standard rigorous result provides a bound on the entanglement growth rate. A Griffiths region is more complicated: although it acts as a weak link in a coarse-grained sense, it is not equivalent to a simple weak bond, and the degrees of freedom within the Griffiths region are strongly coupled. Nevertheless, we show below that the bound can be extended—nonrigorously—to this case by making use of the “ $l$ -bit” picture for many-body localized systems [11,60].

First consider a spin chain in which one bond has a very small coupling. Label the degrees of freedom as in Fig. 10 (left).  $b_1$  and  $b_2$  denote the spins to the left and right of the weak bond respectively, and  $A$  and  $C$  contain the other spins on the left and the right, respectively. The Hamiltonian may be written as

$$H = H_{Ab_1} + H_{b_1b_2} + H_{b_2C}, \quad (42)$$

reflecting the fact that the two sides are coupled only via spins  $b_1$  and  $b_2$ . For example, for an infinite chain with Ising interactions and longitudinal and transverse fields, we would have

$$H_{b_1b_2} = J_{\text{weak}} Z_0 Z_1, \quad (43)$$

$$H_{Ab_1} = \sum_{i < 0} (J Z_{i-1} Z_i + h X_i + g Z_i), \quad (44)$$

$$H_{b_2B} = \sum_{i > 1} (J Z_{i-1} Z_i + h X_i + g Z_i), \quad (45)$$

with  $J_{\text{weak}} \ll J$ . This is a weak link of a simple kind: the systems  $Ab_1$  and  $b_2B$  are coupled only by a small term in the Hamiltonian. In this simple situation there is a rigorous bound on the rate at which entanglement can be generated across the

weak link [61–63]. This bound states that in a pure state

$$\frac{dS_{Ab_1}}{dt} \leq c \|H_{b_1b_2}\| \ln d. \quad (46)$$

Here,  $c$  is a numerical constant given in Ref. [61];  $d$  is the smaller of the Hilbert space dimensions of  $b_1$  and  $b_2$ , here given by  $d = 2$ . Most importantly,  $\|H_{b_1b_2}\|$  is the magnitude of the largest eigenvalue of  $H_{b_1b_2}$ , here equal to  $J_{\text{weak}}$ .

For small  $J_{\text{weak}}$ , the physical rate of entanglement growth (i.e., in a typical state) may be much smaller than the rigorous upper bound (46). Indeed, numerically we find that in a Floquet Ising spin chain the von Neumann entropy growth rate is of order

$$\frac{dS}{dt} \sim J_{\text{weak}}^2 \ln 1/J_{\text{weak}} \quad (47)$$

rather than of order  $J_{\text{weak}}$ , see Sec. VII. But for our purposes in this section the upper bound (46) will suffice.

Microscopically, a Griffiths region does *not* consist of weakly coupled degrees of freedom, so we cannot immediately apply (46). A better cartoon is that the Griffiths region consists of “slow” degrees of freedom. To see this, recall that deep in the MBL phase the Hamiltonian may be formulated in terms of  $l$ -bits—dressed spin variables whose  $Z$  components are strictly conserved [11,60]. This picture is also a useful starting point for considering strongly disordered regions which locally resemble the MBL phase. Since these regions are finite, the dressed spin variables are not strictly conserved, but are instead “slow.”

We can learn how to treat such slow degrees of freedom in the context of a toy model, where the Griffiths region is replaced by a single central spin whose  $Z$  component is almost conserved [see Fig. 10 (right)]. We label the left and right regions by  $A$  and  $C$ , respectively, and the central slow spin by  $b$ . We denote the Pauli operators for the slow spin by  $X, Y, Z$ , and take a Hamiltonian whose  $O(1)$  terms all commute with  $Z$ :

$$H = H_{Ab}(Z) + H_{bC}(Z) + h_{\text{weak}} X. \quad (48)$$

Here the notation  $H_{Ab}(Z)$  means that this term acts on the central spin only via its  $Z$  operator; it can act arbitrarily on the spins in  $A$ . For concreteness, we take the weak term which breaks conservation of  $Z$  to be a transverse field.

It is easy to find an example showing that the *instantaneous* rate of entanglement growth between  $A$  and the rest,  $dS_A/dt$ , can be  $O(1)$ .<sup>7</sup> However, the time-averaged rate is small when  $h_{\text{weak}}$  is small. To see this we relate the physical system to a reference system  $Ab_1b_2C$  in which the spin  $b$  is replaced with two spins. There is a mapping from the Hilbert space of  $AbC$  into that of  $Ab_1b_2C$  given by

$$|\uparrow\rangle_b \rightarrow |\uparrow\rangle_{b_1} |\uparrow\rangle_{b_2}, \quad |\downarrow\rangle_b \rightarrow |\downarrow\rangle_{b_1} |\downarrow\rangle_{b_2} \quad (49)$$

in the  $Z$  basis. This mapping commutes with the time evolution if we choose the following Hamiltonian for the reference system:

$$H_{\text{reference}} = H_{Ab_1}(Z_1) + H_{b_2C}(Z_2) + h_{\text{weak}} X_1 X_2, \quad (50)$$

<sup>7</sup>Take  $C$  to be empty and  $A$  to consist of a single spin, take  $H_{bC}$  to be an Ising coupling, and take the initial state to have both spins polarized in the  $X$  direction.

where  $H_{Ab_1}(Z_1)$  is simply  $H_{Ab}(Z)$  with  $Z$  replaced by  $Z_1$ . Further, if two states  $|\psi\rangle_{\text{phys}}$  and  $|\psi\rangle_{\text{ref}}$  are related by the mapping, they yield the same density matrix on  $A$ . Therefore we are guaranteed that

$$S_A^{\text{phys}}(t) = S_A^{\text{ref}}(t) \quad (51)$$

at all times.

Since the weak field has now become a weak interaction between  $Ab_1$  and  $b_2B$ , we can use Eq. (46) to bound the change  $\Delta S_{Ab_1}$  in the entanglement between  $Ab_1$  and  $b_2B$ :

$$\Delta S_{Ab_1}^{\text{ref}}(t) \leq (c \ln 2) h_{\text{weak}} t. \quad (52)$$

Of course,  $S_{Ab_1}^{\text{ref}}$  is not meaningful in the physical system. But subadditivity of the von Neumann entropy, together with (51), guarantees that it is close to the quantity of interest:  $|S_{Ab_1}^{\text{ref}}(t) - S_A^{\text{phys}}(t)| \leq \ln 2$ . This gives the desired result

$$\Delta S_A^{\text{physical}}(t) \leq (c h_{\text{weak}} t + 2) \ln 2. \quad (53)$$

We see that at long times the time-averaged  $dS_A/dt$  is at most of order  $h_{\text{weak}}$ , and that the coefficient remains of  $O(1)$  even if the size of  $A$  or  $C$  diverges. [See Sec. VII for a numerical analysis of this problem in a Floquet spin chain, showing that the growth rate is even smaller than the maximum allowed by this bound.]

Finally, we turn to a spin chain with subsystems  $ABC$ , where  $B$  is a Griffiths region consisting of a large number  $\ell$  of consecutive spins. We will consider a strongly disordered Griffiths region which locally resembles the fully many body localized phase. Write the Hamiltonian as

$$H = H_A + H_B + H_C + H_{AB} + H_{BC}, \quad (54)$$

where  $H_{AB}$  and  $H_{BC}$  each act on a single bond. Now we make use of the 1-bit picture for the MBL phase [11,60]. We expect that a unitary transformation on  $B$  can reduce its Hamiltonian to a form which only depends on the  $Z_i$  operators for spins  $i \in B$ ,

$$U H_B U^\dagger = H'_B, \quad H'_B = \sum_i h_i Z_i + \sum_{ij} J_{ij} Z_i Z_j + \dots, \quad (55)$$

where the couplings decay exponentially with distance, and where the unitary transformation preserves the locality of operators up to exponential tails. For the purposes of entanglement growth we can work with  $H' = U H U^\dagger$  instead of  $H$ , since  $U$  only introduces  $O(1)$  entanglement.  $H'$  is of the form

$$H' = H_A + H_C + H'_B + U(H_{AB} + H_{BC})U^\dagger. \quad (56)$$

If  $H_{AB} = Z_\alpha Z_\beta$ , where  $\alpha, \beta$  are the boundary spins in  $A$  and  $B$ , respectively,

$$H'_{AB} = U H_{AB} U^\dagger = Z_\alpha \left( \sum_{i \in B} (u_i^X X_i + u_i^Y Y_i + u_i^Z Z_i) + \sum_{i,j \in B} k_{ij}^{ZZ} Z_i Z_j + \dots \right). \quad (57)$$

Now we split the Griffiths region  $B$  into the left-hand, central, and right-hand regions,  $a, b$ , and  $c$ , of length  $\ell/3$  each, and

apply the duplication trick to  $b$  to give a system

$$A a b_1 b_2 c C. \quad (58)$$

We now consider generation of entanglement across the cut  $A a b_1 | b_2 c C$ . The terms in  $H_A$  and  $H_C$  act only within  $A$  or  $C$ , respectively, and can be neglected. Next, we have the terms coming from  $H'_B$ . These act on all the  $Z$ s in  $a, b, c$ . We have some freedom in how we represent these terms, since any  $Z$  in  $b$  can be represented either by a  $Z$  in  $b_1$  or by the corresponding  $Z$  in  $b_2$ . Using this freedom, any term in  $H'_B$  that does not act on *both*  $a$  and  $c$  may be represented with a term which does not cross the cut  $A a b_1 | b_2 c C$ . The largest remaining terms from  $H'_B$ , which act on both  $a$  and  $c$ , are of magnitude  $\sim \exp(-\ell/3\zeta)$ . These terms typically act on  $O(\ell)$  spins in region  $b$  but only  $O(1)$  spins in  $a$  and  $c$ , so can be represented by terms involving only  $O(1)$  spins on one side of the cut and  $O(\ell)$  on the other. Finally, we have the terms from  $H_{AB}$  and  $H_{BC}$  which couple across the boundary of the Griffiths region. After the unitary transformation,  $H_{AB}$  couples the boundary spin  $\alpha$  in region  $A$  to all of the  $l$ -bits in the Griffiths regions, with exponentially decaying couplings. Terms in which  $\alpha$  is coupled to the leftmost spins in region  $b$  are of size  $\sim \exp(-\ell/3\zeta)$ . A term like  $e^{-\ell/3\zeta} Z_\alpha(\dots) X_i$ , where  $i$  is a site in region  $b$ , becomes a coupling involving the corresponding sites in both  $b_1$  and  $b_2$ . Again, these terms involve  $O(\ell)$  spins on one side of the cut and  $O(1)$  on the other.

Altogether, the strongest Hamiltonian terms coupling across the cut  $A a b_1 | b_2 c C$  have size  $\sim e^{-\ell/3\zeta}$  and involve  $O(\ell)$  spins.<sup>8</sup> For a nonrigorous application of the bound (46), we must estimate the norm of the entangling Hamiltonian. This may be larger than  $e^{-\ell/3\zeta}$  by an exponentially large combinatorial factor, since the number of terms is large. We take the region to be sufficiently strongly disordered (i.e.,  $\zeta < \zeta_0$ , where  $\zeta_0$  is an order one constant) that the exponential decay of the couplings wins, giving

$$\frac{dS_{A a b_1}}{dt} \lesssim e^{-\alpha\ell} \quad (59)$$

for some  $\alpha$  that does not depend on  $\ell$ . The difference between  $S_{A a b_1}$  and the physically meaningful entropy  $S_A$  (or  $S_{Aa}$ ) is  $O(\ell)$ , and is unimportant at long times.

This shows that the entanglement growth rate across a strongly disordered Griffiths region is exponentially small in the size of the region, regardless of the size of the complete chain. (Assumptions made in previous work [19,20], where a local timescale associated with the weakest link in a finite chain was taken as the thermalization time of the chain, are equivalent to taking the entanglement growth rate to grow with the size of the adjacent regions. We see this is not the case.) This is enough to show that there is a power law distribution of local rates. In turn this suffices to prove that  $S$  grows subballistically, by the

<sup>8</sup>These terms can be split into two groups, each of which acts on only  $O(1)$  spins from one side. Since (46) can be applied to each group separately and the results added, the appropriate  $\log d$  factor (46) is  $O(1)$  rather than  $O(\ell)$ . In any case, this polynomial correction is negligible in comparison to the error in estimating the coefficient in the exponential.

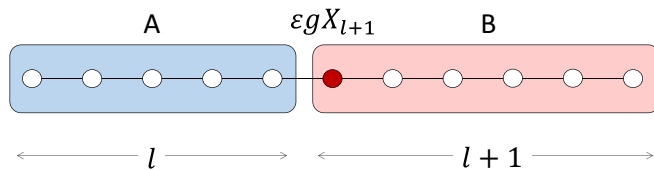


FIG. 11. Setup for the numerical simulation. A chain of  $L = 2l + 1$  spin- $\frac{1}{2}$  degrees of freedom is subjected to Floquet dynamics with Ising couplings and transverse and longitudinal fields. The  $Z$  component of the central spin is almost conserved due to the weak transverse field.

logic in Sec. II. We focused on strongly disordered regions with  $\zeta < \zeta_0$ , while in practice the prevalent weak links with a given  $\Gamma$  may be less strongly disordered. However, this will only decrease the value of the exponent  $a$ .

## VII. ENTANGLING ACROSS A WEAK LINK: NUMERICS

We now present a numerical study of entanglement growth across a microscopic weak link. The setup for the numerical simulation is a spin- $\frac{1}{2}$  chain of length  $L = 2l + 1$ , shown schematically in Fig. 11. We use Floquet dynamics considered previously in Ref. [64]: an Ising spin chain with longitudinal and transverse fields. This system has been shown to thermalize rapidly in the absence of a weak link. A simplifying feature of the Floquet case is that energy is not conserved [64]. We perform exact time evolution using the online package ITENSOR [65].

The weak link we consider is formed by the spin at the central site, whose  $Z$ -component is almost conserved. The commutator of this operator with the one-step time evolution operator is of order  $\epsilon$ , where  $\epsilon$  will be taken to be small. As discussed in Sec. VI, this is a toy model for a Griffiths region: the central spin is an “almost”  $l$ -bit, whereas all other spins are strongly nonconserved under the evolution. The slow spin bottlenecks the growth of entanglement between the rapidly thermalizing regions surrounding it. We focus on the dynamics of the Renyi entropies (including the von Neumann entropy  $S_{vN} \equiv S_1$ )

$$S_n(t) = \frac{1}{1-n} \log_2 \text{Tr} \rho_A^n \quad (60)$$

across the bond connecting the spin at site  $l$  to the nearly conserved spin ( $\rho_A = \text{Tr}_B \rho$  and the regions  $A$  and  $B$  are defined in Fig. 11).

Here we will give results only for the model with a slow spin, but we have also simulated a spin chain with a weak bond. As might be expected from the mapping between a slow spin and a weak link in Sec. VI, the results are extremely similar.

Our main goal will be to validate two key elements of the picture for entanglement growth discussed above. Firstly, that the entanglement growth rate in the vicinity of a weak link,  $x_i$ , can be characterized by a *local* rate  $\Gamma_i$  which is independent of the size of the surrounding regions. Secondly, that in the scaling limit the growth of entanglement entropy is captured by the simple scaling forms discussed in Sec. II. For the present case, the relevant scaling form, if we start from a product state, is

$$S(x, t) = \min\{\Gamma t + |x - x_1|, x, (L - x), v_E t\}, \quad (61)$$

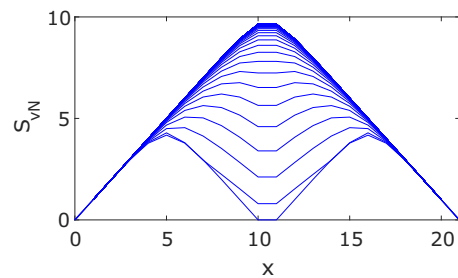


FIG. 12.  $S_{vN}$  as a function of position in systems with  $L = 21$  and  $\epsilon = 0.3$ . The different curves show times from  $t = 0$  to 500 in increments of  $\tau = 10$  (the subsystems are separately entangled prior to  $t = 0$ ).

where  $x_1$  is the location of the weak link. If we start from a state in which the two subsystems are separately fully entangled,

$$S(x, t) = \min\{\Gamma t + |x - x_1|, x, (L - x)\}. \quad (62)$$

In particular, either of these forms implies that for large  $L$  and  $x$ , the entanglement  $S(x_1, t)$  at the location of the weak link has the simple piecewise linear scaling form:

$$S(x_1, t) = \min\{\Gamma_1 t, x_1\}. \quad (63)$$

Although simple, these scaling forms are not *a priori* obvious: they are nontrivial predictions about the universal physics stemming from the results of this paper.

We now give details of the numerical simulation. We use a Floquet time evolution operator

$$U(\epsilon) = U_Z U_X(\epsilon), \quad (64)$$

which includes half a period of evolution with the Ising interactions and longitudinal fields,

$$U_Z = \exp\left(-i\tau \left[ J \sum_{j=1}^{L-1} Z_j Z_{j+1} + h \sum_{j=1}^L Z_j \right]\right), \quad (65)$$

preceded by half a period of evolution with the transverse fields,

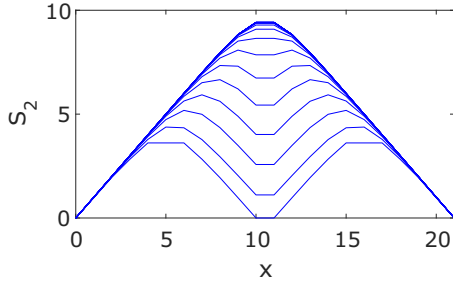
$$U_X(\epsilon) = \exp\left(-i\tau g \left[ \epsilon X_{l+1} + \sum_{j \neq l+1} X_j \right]\right). \quad (66)$$

Note that the transverse field on the central spin is weakened by a (variable) factor  $\epsilon$ . The other couplings are fixed at the values  $J = 1$ ,  $h = 0.809$ ,  $g = 0.9045$ , and  $\tau = 0.8$ , which were shown in Ref. [64] to yield rapid thermalization.

We start from the product state  $|\uparrow \dots \uparrow\rangle$  in the  $Z$  basis. But before beginning the entangling dynamics, we evolve the left and right subsystems separately, i.e., with  $\epsilon = 0$ , for a time  $T_0$  to ensure that they are separately strongly entangled. In the simulations, we have used  $T_0 = 5$ , however, we note that our results depend very weakly on  $T_0$ . The state at time  $t \geq 0$  is therefore defined to be

$$|\psi(t)\rangle = U(\epsilon)^t U(0)^{T_0} |\uparrow \dots \uparrow\rangle. \quad (67)$$

Note that the entanglement between  $A$  and  $B$  is zero when  $t = 0$ . In Fig. 12, we plot a typical spatial dependence of  $S_{vN}(x, t)$  for a system of size  $L = 21$  and for successive times  $t$  starting from  $t = 0$ . Figure 13 shows the same for  $S_2(x, t)$ .


 FIG. 13. As Fig. 12, but for the second Renyi entropy  $S_2$ .

Let us now examine the validity of the scaling forms. In Fig. 14, we plot the von Neumann and second Renyi entropies, rescaled by their asymptotic late time values, against the rescaled time variable  $\Gamma_n t / S_{\max}$ . Here,  $\Gamma_n$  is the growth rate of  $S_n(t)$  obtained by fitting the linear growth near  $t = 0$  for  $L = 21$ .  $S_{\max}$  is the value of the entropy as  $t \rightarrow \infty$ , which is determined numerically and which depends on  $n$  and  $L$ . We note that in the case of the von Neumann entropy  $S_{\max}$  converges very quickly with increasing  $L$  to the prediction of Ref. [33] for a random state.

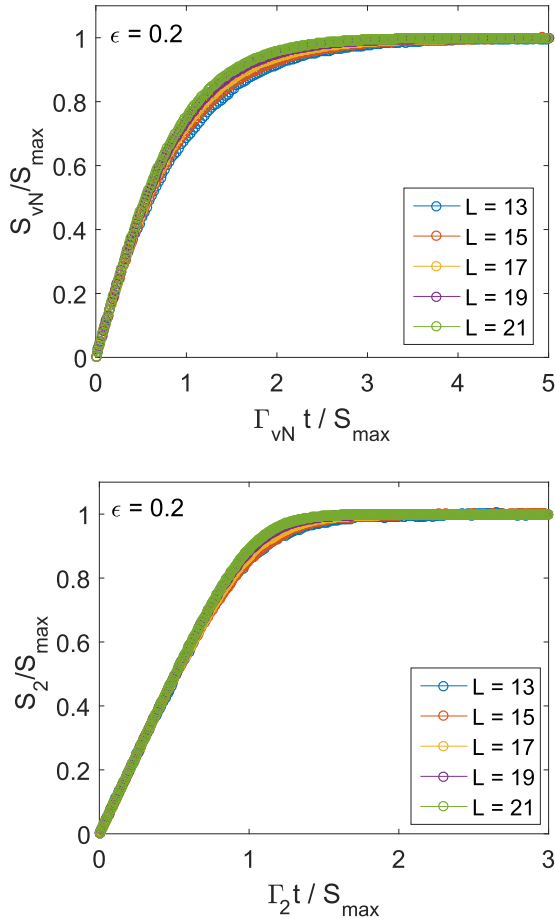


FIG. 14. The von Neumann (top) and second Renyi (bottom) entropies scaled by their maximal value at large time  $S_{\max}$  vs the rescaled time  $\Gamma_n t / S_{\max}$  for different values of  $L$  and for  $\epsilon = 0.2$ . The value of  $S_{\max}$  is determined numerically.

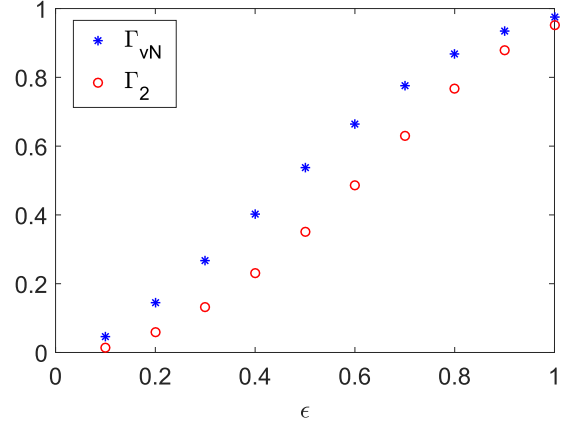


FIG. 15. The initial growth rates  $\Gamma_n$  as a function of  $\epsilon$  (calculated using  $L = 21$ ). The stars (blue) and circles (red) correspond to von Neumann and second Renyi entropy, respectively.

It is clear from Fig. 14 that the early time growth rate,  $\Gamma_n$ , is independent of the length of the system. This is consistent with our coarse-grained picture. By numerically fitting the data, we find that for small  $\epsilon < 0.1$  the growth rates are given by

$$\Gamma_{\text{vN}} = A_{\text{vN}} \epsilon^2 \log_2 \frac{B}{\epsilon}, \quad \Gamma_n = \frac{An}{n-1} \epsilon^2, \quad (68)$$

where  $A_{\text{vN}}$ ,  $B$ , and  $A$  are  $\epsilon$ -independent constants. The rates for larger values of  $\epsilon = 0.1, 0.2, \dots, 1$  are shown in Fig. 15. This confirms that indeed the growth rate is small in  $\epsilon$  and that a nearly conserved quantity causes a bottleneck for entanglement growth. Note that for small  $\epsilon$ , the growth rate is parametrically smaller than the rigorous upper bound in Sec. VI. Interestingly, Fig. 15 suggests that for  $\epsilon = 1$  (the homogeneous case) the growth rates for  $S_{\text{vN}}$  and  $S_2$  may be equal.

We also find that the transition from linear growth to saturation becomes sharper with increasing  $L$ , consistent with the expected scaling form Eq. (63). This is much clearer for the second and higher Renyi entropies (Fig. 14). For the von Neumann entropy, a more careful finite size analysis is required, which we give below.

For translationally invariant Floquet systems with no conserved quantities, the late time saturation of the entropy has been found to be exponential [64]. We also obtain a good fit at late times with

$$S_{\text{vN}} = S_{\max} - \Delta(t), \quad \Delta(t) = \exp(-\Gamma' |t - t_*|), \quad (69)$$

where the parameters  $\Gamma'$  and  $t_*$  of the fit are extracted separately for each  $L$  and  $\epsilon$ . We find that at small  $\epsilon$  the saturation rate  $\Gamma'$  behaves as

$$\Gamma' = A' \epsilon^2. \quad (70)$$

The timescale  $t_*$  for saturation is of order  $L$ .

Assume that there is a simple crossover between linear and exponential behavior at a time  $t_l$ . Matching  $S$  and  $\partial S / \partial t$  at this time gives the following gluing conditions:

$$t_l = \frac{S_{\max}}{\Gamma_{\text{vN}}} - \frac{1}{\Gamma'}, \quad t_* = t_l + \frac{1}{\Gamma'} \log_2 \frac{\Gamma_{\text{vN}}}{\Gamma'}, \quad (71)$$

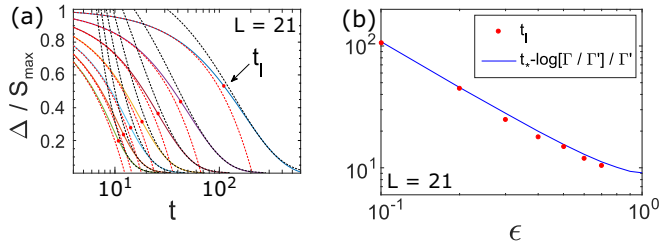


FIG. 16. (a) The *solid* lines show the normalized deviation from maximal entropy  $\Delta/S_{\max}$  defined in Eq. (69) vs time  $t$ . The different colors correspond to different values of  $\epsilon$  ranging between 0.1, 0.2, ..., 0.7. The *dashed* curves are the fits to the linear form:  $1 - \Gamma t/S_{\max}$  (red dashed) and to the exponential form:  $1 - \exp[-\Gamma'(t - t_*)]/S_{\max}$  (black dashed). The red dots mark the *crossover points* between linear behavior, at short times, and exponential, at long times. These crossover points are used to extract the timescale  $t_l$  is extracted. (b) Comparison between the extracted crossover time  $t_l$  (red dots) and the expected form Eq. (71) (blue solid curve).

which means that

$$S(t_l) = S_{\max} - \Gamma_{vN}/\Gamma'. \quad (72)$$

In Fig. 16, we test the assumption underlying the previous. In the first panel, we present the linear (red dashed lines) and exponential (black dashed lines) fits to  $\Delta(t)/S_{\max}$ . The red dots are crossover times between these two behaviors, determined by eye. In the second panel, we compare these crossover times with the prediction in Eq. (71), finding good agreement.

The previous equation shows that the departure from linear behavior occurs when the entropy is within

$$\Delta S_{vN} \sim \frac{\Gamma_{vN}}{\Gamma'} \sim \frac{A_{vN}}{A'} \log_2 \frac{B}{\epsilon} \quad (73)$$

bits of its maximum. The  $\Delta S \sim \log_2 1/\Gamma$  behavior for the von Neumann entropy indicates that the finite-size rounding is more severe for weaker weak links; this conforms with what we find numerically. For the higher Renyi entropies, this logarithmic factor is absent, as a result of Eq. (68). Since  $\Delta S$  is independent of  $L$ , the above confirms the scaling form Eq. (63) for a system of size  $L$  with a weak link whose strength is fixed as  $L \rightarrow \infty$ . (The deviation from linearity for the last  $\Delta S \sim \log_2 1/\Gamma$  bits of entanglement is also negligible if we take  $\Gamma$  to scale as a negative power of  $L$ , which is the natural scaling in the Griffiths regime.)

Note that if the relative logarithmic factor in the growth rates for  $S_{vN}$  and  $S_{n>1}$  [Eq. (68)] also applies for coarse-grained weak links, then the von Neumann entropy in the Griffiths phase will exceed the higher Renyi entropies by a factor of order  $\log t$  at late times (since the weak links that are relevant at time  $t$  have strength  $\Gamma \sim t^{-1/(2+a)}$ ).

We have confirmed the two key assumptions:  $\Gamma_n$  is independent of  $L$ , and the scaling form Eq. (6) is indeed obtained in the large  $L$  limit for a microscopic weak link. If we allow ourselves to extrapolate the above results to Griffiths regions (coarse-grained weak links), these conclusions support the scaling forms derived from the surface growth picture.

## VIII. SUMMARY

We have examined the dynamics of isolated one-dimensional quantum systems that thermalize, but have a distribution of weak links produced by quenched randomness. This occurs in systems that sustain (but which are outside) the many-body-localized (MBL) phase, due to Griffiths regions that are locally in this phase. We developed coarse-grained pictures for the production of entanglement and the spreading of operators and of conserved densities.

We found that such systems have multiple dynamic length scales that diverge with different powers of the time. These length scales are for the growth of entanglement, the spreading of conserved densities, the spreading of initially local operators, and the width of the “front” of a spreading operator. These quantities have effective classical dynamics of distinct types. Entanglement growth maps to classical surface growth with inhomogeneous rates. Transport of conserved quantities is governed by random walk dynamics with weak links. Finally, the front of a growing operator can be related to the passage of a biased random walk through weak links.

Contrary to systems without quenched disorder, the process of entanglement saturation (either for states or operators) is always parametrically slower than the spreading of operators as measured by the norm of their commutator with a local operator or by the out-of-time-order correlator (OTOC). Entanglement growth is subballistic even in the weak-disorder portion of the Griffiths phase: sub-ballistic growth is inevitable whenever weak links of arbitrary length can be created, no matter how small the probability is for such weak links. By contrast, when weak links are sufficiently rare, both the OTOC and conserved densities are relatively insensitive to them: there is a regime where conserved quantities spread diffusively and the operators spread ballistically, as in a clean nonintegrable chain.

We also examined the exchange of quantum information between two clean systems coupled by a single weak link, giving universal scaling forms for the growth of entanglement and the spreading of operators from one system into the other.

Various questions remain for the future. Each of the quantities we have considered (entanglement, the OTOC, and conserved densities) is affected by weak links with a power law distribution of timescales (with exponent denoted  $a$  in the text). An important task is to clarify the relations between the exponents  $a$  for distinct quantities, as discussed in Sec. IV. For example, the exponents  $a_C$  pertaining to conserved quantities may differ between different conserved quantities, as suggested by recent numerics [58] (this issue could also be probed with the methods of Refs. [54,66]). In a system with conserved energy, can the exponent  $a$  for entanglement exceed  $a_{\text{energy}}$  for energy?

It has been suggested on the basis of simulations [67] that subballistic entanglement growth may occur in the thermal phase of 1D chains with quasiperiodic detuning rather than disorder. The relation of such systems to rare-region physics remains to be understood.

The pictures described here are set up to deal with dynamics in the thermal phase. It would be interesting to understand the crossover effects at the MBL phase transition [19,20,68–71] in more detail by relating the present considerations to

real-space RG approaches. The results above are expected to apply at sufficiently large length and timescales no matter how close the system is to the MBL transition; however, the scales required will diverge as the MBL transition is approached. It may also be interesting to consider a coarse-grained treatment of the network of locally *thermal* Griffiths regions in the MBL phase. In higher dimensions, such rare regions have been argued to destabilize the MBL phase [72,73].

## ACKNOWLEDGMENTS

We thank S. Gopalakrishnan, J. Haah, C. Jonay, and S. Vijay for collaboration on related work. AN acknowledges support from the Gordon and Betty Moore Foundation under the EPiQS initiative (grant No. GBMF4303) and from EPSRC Grant No. EP/N028678/1. JR acknowledges a fellowship from the Gordon and Betty Moore Foundation under the EPiQS initiative (Grant No. GBMF4303).

- 
- [1] P. Calabrese and J. Cardy, Evolution of entanglement entropy in one-dimensional systems, *J. Stat. Mech.* (2005) P04010.
- [2] G. De Chiara, S. Montangero, P. Calabrese, and R. Fazio, Entanglement entropy dynamics of Heisenberg chains, *J. Stat. Mech.: Theor. Exp.* (2006) P03001.
- [3] M. Žnidarič, T. Prosen, and P. Prelovšek, Many-body localization in the Heisenberg  $xxz$  magnet in a random field, *Phys. Rev. B* **77**, 064426 (2008).
- [4] J. H. Bardarson, F. Pollmann, and J. E. Moore, Unbounded Growth of Entanglement in Models of Many-Body Localization, *Phys. Rev. Lett.* **109**, 017202 (2012).
- [5] H. Kim and D. A. Huse, Ballistic Spreading of Entanglement in a Diffusive Nonintegrable System, *Phys. Rev. Lett.* **111**, 127205 (2013).
- [6] A. Nahum, J. Ruhman, S. Vijay, and Jeongwan Haah, Quantum Entanglement Growth Under Random Unitary Dynamics, *Phys. Rev. X* **7**, 031016 (2017).
- [7] R. Nandkishore and D. A. Huse, Many-body localization and thermalization in quantum statistical mechanics, *Annu. Rev. Condens. Matter Phys.* **6**, 15 (2015).
- [8] E. H. Lieb and D. W. Robinson, The finite group velocity of quantum spin systems, *Commun. Math. Phys.* **28**, 251 (1972).
- [9] D. A. Roberts, D. Stanford, and L. Susskind, Localized shocks, *J. High Energy Phys.* **03** (2015) 51.
- [10] M. Serbyn, Z. Papić, and D. A. Abanin, Universal Slow Growth of Entanglement in Interacting Strongly Disordered Systems, *Phys. Rev. Lett.* **110**, 260601 (2013).
- [11] D. A. Huse, R. Nandkishore, and V. Oganesyan, Phenomenology of fully many-body-localized systems, *Phys. Rev. B* **90**, 174202 (2014).
- [12] Y. Huang, Y.-L. Zhang, and X. Chen, Out-of-time-ordered correlators in many-body localized systems, *Ann. der Phys.* **529**, 1600318 (2017).
- [13] R. Fan, P. Zhang, H. Shen, and H. Zhai, Out-of-time-order correlation for many-body localization, *Sci. Bull.* **62**, 707 (2017).
- [14] Y. Chen, Universal logarithmic scrambling in many body localization, [arXiv:1608.02765](https://arxiv.org/abs/1608.02765) [cond-mat.dis-nn].
- [15] B. Swingle and D. Chowdhury, Slow scrambling in disordered quantum systems, *Phys. Rev. B* **95**, 060201 (2017).
- [16] R.-Q. He and Z.-Y. Lu, Characterizing many-body localization by out-of-time-ordered correlation, *Phys. Rev. B* **95**, 054201 (2017).
- [17] X. Chen, T. Zhou, D. A. Huse, and E. Fradkin, Out-of-time-order correlations in many-body localized and thermal phases, *Ann. der Phys.* **529**, 1600332 (2017).
- [18] K. Slagle, Z. Bi, Y.-Z. You, and C. Xu, Out-of-time-order correlation in marginal many-body localized systems, *Phys. Rev. B* **95**, 165136 (2017).
- [19] R. Vosk, D. A. Huse, and E. Altman, Theory of the Many-Body Localization Transition in One-Dimensional Systems, *Phys. Rev. X* **5**, 031032 (2015).
- [20] A. C. Potter, R. Vasseur, and S. A. Parameswaran, Universal Properties of Many-Body Delocalization Transitions, *Phys. Rev. X* **5**, 031033 (2015).
- [21] K. Agarwal, S. Gopalakrishnan, M. Knap, M. Müller, and E. Demler, Anomalous Diffusion and Griffiths Effects Near the Many-Body Localization Transition, *Phys. Rev. Lett.* **114**, 160401 (2015).
- [22] Y. Bar Lev, G. Cohen, and D. R. Reichman, Absence of Diffusion in an Interacting System of Spinless Fermions on a One-Dimensional Disordered Lattice, *Phys. Rev. Lett.* **114**, 100601 (2015).
- [23] D. J. Luitz, N. Laflorencie, and F. Alet, Extended slow dynamical regime close to the many-body localization transition, *Phys. Rev. B* **93**, 060201 (2016).
- [24] I. Khait, S. Gazit, N. Y. Yao, and A. Auerbach, Spin transport of weakly disordered Heisenberg chain at infinite temperature, *Phys. Rev. B* **93**, 224205 (2016).
- [25] M. Žnidarič, A. Scardicchio, and V. K. Varma, Diffusive and Subdiffusive Spin Transport in the Ergodic Phase of a Many-Body Localizable System, *Phys. Rev. Lett.* **117**, 040601 (2016).
- [26] H. P. Lüschen, P. Bordia, S. Scherg, F. Alet, E. Altman, U. Schneider, and I. Bloch, Evidence for Griffiths-Type Dynamics Near the Many-Body Localization Transition in Quasi-Periodic Systems, *Phys. Rev. Lett.* **119**, 260401 (2017).
- [27] D. J. Luitz and Y. B. Lev, Information propagation in isolated quantum systems, *Phys. Rev. B* **96**, 020406 (2017).
- [28] A. Chandran, V. Khemani, C. R. Laumann, and S. L. Sondhi, Many-body localization and symmetry-protected topological order, *Phys. Rev. B* **89**, 144201 (2014).
- [29] A. C. Potter and R. Vasseur, Symmetry constraints on many-body localization, *Phys. Rev. B* **94**, 224206 (2016).
- [30] I. V. Protopopov, W. W. Ho, and D. A. Abanin, The effect of  $SU(2)$  symmetry on many-body localization and thermalization, *Phys. Rev. B* **96**, 041122 (2017).
- [31] A. Nahum, S. Vijay, and J. Haah, Operator Spreading in Random Unitary Circuits, *Phys. Rev. X* **8**, 021014 (2018).
- [32] C. W. von Keyserlingk, T. Rakovszky, F. Pollmann, and S. L. Sondhi, Operator Hydrodynamics, OTOCs, and Entanglement Growth in Systems Without Conservation Laws, *Phys. Rev. X* **8**, 021013 (2018).
- [33] D. N. Page, Average Entropy of a Subsystem, *Phys. Rev. Lett.* **71**, 1291 (1993).
- [34] T. Zhou and D. J. Luitz, Operator entanglement entropy of the time evolution operator in chaotic systems, *Phys. Rev. B* **95**, 094206 (2017).

- [35] P. Meakin, P. Ramanlal, L. M. Sander, and R. C. Ball, Ballistic deposition on surfaces, *Phys. Rev. A* **34**, 5091 (1986).
- [36] M. Kardar, G. Parisi, and Y-C. Zhang, Dynamic Scaling of Growing Interfaces, *Phys. Rev. Lett.* **56**, 889 (1986).
- [37] J. Krug and T. Halpin-Healy, Directed polymers in the presence of columnar disorder, *J. de Physique I* **3**, 2179 (1993).
- [38] AI Larkin and Yu N Ovchinnikov, Quasiclassical method in the theory of superconductivity, *Sov. Phys. JETP* **28**, 1200 (1969).
- [39] A. Kitaev, Hidden Correlations in the Hawking Radiation and Thermal Noise, talk given at Fundamental Physics Prize Symposium, November 10, 2014, <https://breakthroughprize.org/Laureates/1/L3>.
- [40] S. H. Shenker and D. Stanford, Black holes and the butterfly effect, *J. High Energy Phys.* **03** (2014) 67.
- [41] S. H. Shenker and D. Stanford, Multiple shocks, *J. High Energy Phys.* **12** (2014) 46.
- [42] J. Maldacena, S. H. Shenker, and D. Stanford, A bound on chaos, *J. High Energy Phys.* **08** (2016) 106.
- [43] I. L. Aleiner, L. Faoro, and Lev B. Ioffe, Microscopic model of quantum butterfly effect: Out-of-time-order correlators and traveling combustion waves, *Ann. Phys.* **375**, 378 (2016).
- [44] A. A. Patel and S. Sachdev, Quantum chaos on a critical Fermi surface, *Proc. Natl. Acad. Sci. USA* **114**, 1844 (2017).
- [45] D. Chowdhury and B. Swingle, Onset of many-body chaos in the  $o(n)$  model, *Phys. Rev. D* **96**, 065005 (2017).
- [46] A. A. Patel, D. Chowdhury, S. Sachdev, and B. Swingle, Quantum Butterfly Effect in Weakly Interacting Diffusive Metals, *Phys. Rev. X* **7**, 031047 (2017).
- [47] D. Stanford, Many-body chaos at weak coupling, *J. High Energy Phys.* **10** (2016) 009.
- [48] S. Banerjee and E. Altman, Solvable model for a dynamical quantum phase transition from fast to slow scrambling, *Phys. Rev. B* **95**, 134302 (2017).
- [49] Y. Gu, X.-L. Qi, and D. Stanford, Local criticality, diffusion and chaos in generalized sachdev-ye-kitaev models, *J. High Energy Phys.* **05** (2017) 125.
- [50] D. A. Roberts and B. Swingle, Lieb-Robinson Bound and the Butterfly Effect in Quantum Field Theories, *Phys. Rev. Lett.* **117**, 091602 (2016).
- [51] D. A Roberts and D. Stanford, Diagnosing Chaos using Four-Point Functions in Two-Dimensional Conformal Field Theory, *Phys. Rev. Lett.* **115**, 131603 (2015).
- [52] B. Dóra and R. Moessner, Out-of-Time-Ordered Density Correlators in Luttinger Liquids, *Phys. Rev. Lett.* **119**, 026802 (2017).
- [53] A. Bohrdt, C. B. Mendl, M. Endres, and M. Knap, Scrambling and thermalization in a diffusive quantum many-body system, *New J. Phys.* **19**, 063001 (2017).
- [54] E. Leviatan, F. Pollmann, J. H. Bardarson, D. A. Huse, and E. Altman, Quantum thermalization dynamics with matrix-product states, [arXiv:1702.08894](https://arxiv.org/abs/1702.08894).
- [55] Wen Wei Ho and Dmitry A. Abanin, Entanglement dynamics in quantum many-body systems, *Phys. Rev. B* **95**, 094302 (2017).
- [56] Márk Mezei and Douglas Stanford, On entanglement spreading in chaotic systems, *J. High Energy Phys.* **05** (2017) 065.
- [57] C. Jonay, D. A. Huse, and A. Nahum, Coarse-grained dynamics of operator and state entanglement, [arXiv:1803.00089](https://arxiv.org/abs/1803.00089).
- [58] J. J. Mendoza-Arenas, M. Znidaric, V. K. Varma, J. Goold, S. R. Clark, and A. Scardicchio, Asymmetry in energy versus spin transport in certain interacting, disordered systems, [arXiv:1803.11555](https://arxiv.org/abs/1803.11555).
- [59] M. Schulz, S. R. Taylor, C. A. Hooley, and A. Scardicchio, Energy transport in a disordered spin chain with broken U(1) symmetry: Diffusion, subdiffusion, and many-body localization, [arXiv:1805.01036](https://arxiv.org/abs/1805.01036).
- [60] M. Serbyn, Z. Papić, and D. A. Abanin, Local Conservation Laws and the Structure of the Many-Body Localized States, *Phys. Rev. Lett.* **111**, 127201 (2013).
- [61] Karel Van Acoleyen, Michaël Mariën, and Frank Verstraete, Entanglement Rates and Area Laws, *Phys. Rev. Lett.* **111**, 170501 (2013).
- [62] K. M. R. Audenaert, Quantum skew divergence, *J. Math. Phys.* **55**, 112202 (2014).
- [63] S. Bravyi, Upper bounds on entangling rates of bipartite hamiltonians, *Phys. Rev. A* **76**, 052319 (2007).
- [64] Liangsheng Zhang, Hyungwon Kim, and David A Huse, Thermalization of entanglement, *Phys. Rev. E* **91**, 062128 (2015).
- [65] ITENSOR, <http://itensor.org>.
- [66] C. D. White, M. Zaletel, Roger S. K. Mong, and G. Refael, Quantum dynamics of thermalizing systems, *Phys. Rev. B* **97**, 035127 (2018).
- [67] Y. Bar Lev, D. M. Kennes, C. Klöckner, D. R Reichman, and C. Karrasch, Transport in quasiperiodic interacting systems: From superdiffusion to subdiffusion, *Europhys. Lett.* **119**, 37003 (2017).
- [68] V. Khemani, S. P. Lim, D. N. Sheng, and D. A. Huse, Critical Properties of the Many-Body Localization Transition, *Phys. Rev. X* **7**, 021013 (2017).
- [69] P. T. Dumitrescu, R. Vasseur, and A. C. Potter, Scaling Theory of Entanglement at the Many-Body Localization Transition, *Phys. Rev. Lett.* **119**, 110604 (2017).
- [70] T. Thiery, F. Huveneers, M. Müller, and W. D. Roeck, Many-body delocalization as a quantum avalanche, [arXiv:1706.09338](https://arxiv.org/abs/1706.09338).
- [71] T. Thiery, Markus Müller, and Wojciech De Roeck, A microscopically motivated renormalization scheme for the MBL/ETH transition, [arXiv:1711.09880](https://arxiv.org/abs/1711.09880).
- [72] W. De Roeck and F. Huveneers, Stability and instability towards delocalization in many-body localization systems, *Phys. Rev. B* **95**, 155129 (2017).
- [73] W. D. Roeck and J. Z. Imbrie, Many-body localization: Stability and instability, *Phil. Trans. R. Soc. A* **375**, 20160422 (2017).